Mixing, Chemical Reaction, and Flowfield Development in Ducted Rockets

S. P. Vanka*
Argonne National Laboratory, Argonne, Illinois
and
R. R. Craig† and F. D. Stull‡
Air Force Wright Aeronautical Laboratories, Wright-Patterson AFB, Ohio

Calculations have been made of the three-dimensional mixing, chemical reaction, and flowfield development in a typical ducted rocket configuration. The governing partial differential equations are numerically solved by an iterative finite-difference solution procedure. The physical models include the $k-\epsilon$ turbulence model, one-step reaction, and mixing controlled chemical reaction rate. Radiation is neglected. The mean flow structure, fuel dispersal patterns, and temperature field are presented in detail for a base configuration with a 0.058 m dome height, 45-deg side-arm inclination, and with gaseous ethylene injected from the dome plate at an eccentric location. In addition, the influences of the geometrical parameters, such as dome height, inclination of the side arms, and location of the fuel injector, are studied.

Nomenclature

a,b,c = parameters in the relation for specific heats
A_p, A_n = finite-difference coefficients
C_p = specific heat
C_1, C_2, C_μ = constants in the turbulence model
C_{g1}, C_{g2} = constants in the concentration fluctuation equation
f = nondimensional mixture fraction
g = concentration fluctuation
H_{fu} = heat of reaction
h = stagnation enthalpy
i = stoichiometric ratio
k = turbulence kinetic energy
M = molecular weight
m = mass fraction
P = production of turbulence kinetic energy
P_g = production of concentration fluctuations
p = pressure
R = gas constant
r = radial coordinate
S = source term, $= S^u + S^p\phi$
$\Lambda^\eta, \Lambda^\iota$ = components of source term
T = temperature
u,v,w = velocity components in x,r,θ directions, respectively
x = axial coordinate
α = underrelaxation factor
β = proportion of time spent in f_+ state
Γ = exchange coefficient
ϵ = rate of dissipation of kinetic energy of turbulence
θ = angular coordinate
μ_{eff} = effective viscosity, $= \mu_t + \mu_\ell$
μ_ℓ = laminar viscosity
μ_t = turbulent viscosity
ρ = density
σ = turbulent Prandtl/Schmidt number
Φ = $m_{fu} - m_{ox}/i$
ϕ = general flow variable

Subscripts

A = airstream
f = mixture fraction
fu = fuel
F = fuel stream
g = concentration fluctuation
k = turbulence kinetic energy
ox = oxidant
pr = product
u,v,w = velocities in x,r,θ directions, respectively
ϵ = rate of dissipation of k
$+,-$ = positive and negative sides of fluctuation

I. Introduction

A DUCTED rocket is a ramjet variant with a configuration such as that shown in Fig. 1. Gaseous fuel from a gas generator is injected through the dome plate and the air is supplied through two side arms attached to the combustor periphery. The side arms are inclined with the duct axis located symmetrically in the azimuth direction. The mixing of the fuel and airstreams occurs in a complex flowfield formed by the two flow streams. The complex flow recirculation patterns in the dome region and behind the airstream aid in stabilizing the combustion process. A detailed understanding of the aerodynamics and fuel-air mixing processes in such a configuration is necessary for improving the combustion efficiency and the thrust produced by the ducted rocket. The geometrical variables (such as the angle of the side arms, length of the combustor, distance between the dome plate and the side arms, and location of the fuel injector) may then be optimized for maximum efficiency and thrust.

Numerous flow complexities exist in the ducted rocket configuration. The side entry of the airstream sets up a complex three-dimensional flow pattern, consisting of a pair of vortices in the cross-sectional plane and a complex recirculation pattern in the dome region. The flow is often high-speed with a

Received May 5, 1985; presented as Paper 85-1271 at the 21st AIAA/ASME/SAE Joint Propulsion Conference, Monterey, CA, July 8-10, 1985; revision received Feb. 5, 1986.

*Engineer. Member AIAA.
†Aerospace Engineer.
‡Supervisory Aerospace Engineer. Associate Fellow AIAA.

choked fuel jet at the dome. The shear layers and the regions of impingement of the airstreams are characterized by intense turbulence and mixing; very little is known of the turbulence-chemistry interactions in such a complex three-dimensional flowfield. In addition, in a practical ducted rocket, the gas generator effluent has a complex composition that could significantly influence the transient processes such as ignition and flame blowout.

There have been very few studies, experimental or analytical, of the detailed combustion processes inside the ducted rocket. In a continuing investigation, flow-visualization studies are being made at Wright-Patterson AFB, Ohio, to characterize the isothermal flowfields. Studies made thus far[1,2] have indicated the presence of complex vortex patterns and multiple recirculation regions, especially in the dome region. Vanka et al.[3] have reproduced some of these flow patterns in an analytical study by numerically solving the partial differential equations governing the steady three-dimensional isothermal fluid flow. Calculations were made for different side-arm angles and different dome heights. This preliminary study demonstrated the utility of a computational tool in understanding the ducted rocket combustion processes.

The combustion efficiencies for a ducted rocket configuration with gaseous ethylene injected from the dome are currently being investigated in a thrust stand at the Air Force Wright Aeronautical Laboratories for different fuel-air ratios and combustor lengths. These tests are aimed primarily at acquiring the gross features and, thus, do not provide the complete details of the combustion processes and flowfields. Recently, Chen and Tao[4] simplified the ducted rocket geometry to be axisymmetric and numerically solved the two-dimensional reacting flow equations. Because of the axisymmetric approximation, the study of Chen and Tao[4] does not reveal the vortex structures observed in the water-tunnel experiments.[1,2] Also, their study neglects the circumferential nonuniformities and transport, and, therefore, inaccurately represents the flow and combustion processes.

The present study has been undertaken to analytically study the characteristics of the three-dimensional reacting flowfield in ducted rocket configurations. In this study, equations governing the fully elliptic three-dimensional reacting flow have been solved numerically by an iterative finite-difference algorithm. For simplicity, the combustion process is assumed to occur in a one-step infinitely fast chemical reaction, represented as

$$1\text{ kg fuel} + i\text{ kg oxidant} = (1+i)\text{ kg products} \tag{1}$$

where i is the stoichiometric oxidant-to-fuel ratio. The chemical reaction is taken to be mixing-limited, and fuel and oxidant are assumed to react instantaneously. The wall heat losses are neglected and the flow is considered to be adiabatic. The effects of turbulence are represented through a turbulence model in which a scalar eddy viscosity is calculated from two local turbulence variables. In the current work, the $(k\sim\epsilon)$ turbulence model[5] has been used and partial differential equations are solved for the transport of the kinetic energy of turbulence, k, and its dissipation rate, ϵ. Radiation is neglected. These simplifications have been made primarily to capture the important features of the flow without extensive computation. In the present work, calculations also have been made for different geometrical parameters to study their influence on flowfield development and mixing efficiency.

The present numerical study is being complemented with an experimental investigation utilizing a combustor thrust stand.[2] Both gaseous and liquid fuel are combusted and the combustion efficiencies with different geometrical parameters are being investigated. For the present calculations, recent tests with gaseous ethylene injection from the dome plate have been considered as the base configuration. The injection port is a simple orifice 0.01524 m (0.6 in.) in diameter located in the dome plate at 0.0381 m below the combustor centerline on the bisector of the angle between the two inlet arms. The test conditions are: airflow, 1.814 kgs; air temperature, 556 K; and fuel flow rate, 0.1088 kg/s. Two combustor lengths of 0.762 and 0.4572 m have been considered. The measured combustion efficiencies are compared with the calculations.

The following sections describe the details of the current calculations. The governing equations are given in Sec. II, and the solution algorithm is described briefly in Sec. III. The results of the calculations for the base configuration are given in Sec. IV. In Sec. V, the effects of varying the side-arm angle, dome height, and location of the fuel injector are investigated.

II. Governing Equations

The ducted rocket geometry is conveniently described in the cylindrical polar coordinate system. The airflow from the side arms is prescribed as a boundary condition to the flow domain; consequently, the flow in the side arms is not analyzed. Because flow recirculation is in all three space directions, the fully elliptic, three-dimensional, steady-state Navier-Stokes equations given below are solved.

Mass continuity:

$$\frac{\partial}{\partial x}(\rho u)+\frac{\partial}{r\partial r}(r\rho v)+\frac{\partial}{r\partial\theta}(\rho w)=0 \tag{2}$$

x momentum:

$$\frac{\partial}{\partial x}(\rho uu)+\frac{\partial}{r\partial r}(r\rho vu)+\frac{\partial}{r\partial\theta}(\rho wu)=-\frac{\partial p}{\partial x}+\frac{\partial}{\partial x}\left(\mu_{\text{eff}}\frac{\partial u}{\partial x}\right)+\frac{\partial}{r\partial r}\left(r\mu_{\text{eff}}\frac{\partial u}{\partial r}\right)+\frac{\partial}{r\partial\theta}\left(\mu_{\text{eff}}\frac{\partial u}{r\partial\theta}\right)+S_u \tag{3}$$

r momentum:

$$\frac{\partial}{\partial x}(\rho uv)+\frac{\partial}{r\partial r}(r\rho vv)+\frac{\partial}{r\partial\theta}(\rho wv)=-\frac{\partial p}{\partial r}+\frac{\partial}{\partial x}\left(\mu_{\text{eff}}\frac{\partial v}{\partial x}\right)+\frac{\partial}{r\partial r}\left(r\mu_{\text{eff}}\frac{\partial v}{\partial r}\right)+\frac{\partial}{r\partial\theta}\left(\mu_{\text{eff}}\frac{\partial v}{r\partial\theta}\right)+S_v \tag{4}$$

θ momentum:

$$\frac{\partial}{\partial x}(\rho uw)+\frac{\partial}{r\partial r}(r\rho vw)+\frac{\partial}{r\partial\theta}(\rho ww)=-\frac{\partial p}{r\partial\theta}+\frac{\partial}{\partial x}\left(\mu_{\text{eff}}\frac{\partial w}{\partial x}\right)+\frac{\partial}{r\partial r}\left(r\mu_{\text{eff}}\frac{\partial w}{\partial r}\right)+\frac{\partial}{r\partial\theta}\left(\mu_{\text{eff}}\frac{\partial w}{r\partial\theta}\right)+S_w \tag{5}$$

The turbulent diffusional fluxes are calculated from a two-equation $(k\sim\epsilon)$ turbulence model. The additional equations solved are:

Kinetic energy of turbulence (k):

$$\frac{\partial}{\partial x}(\rho uk)+\frac{\partial}{r\partial r}(\rho rvk)+\frac{\partial}{r\partial\theta}(\rho wk)=-\frac{\partial}{\partial x}\left(\Gamma_k\frac{\partial k}{\partial x}\right)+\frac{\partial}{\partial r}\left(r\Gamma_k\frac{\partial k}{\partial r}\right)+\frac{\partial}{r\partial\theta}\left(\Gamma_k\frac{\partial k}{r\partial\theta}\right)+P-\rho\epsilon \tag{6}$$

Dissipation rate of k:

$$\frac{\partial}{\partial x}(\rho u\epsilon)+\frac{\partial}{r\partial r}(\rho rv\epsilon)+\frac{\partial}{r\partial\theta}(\rho w\epsilon)=\frac{\partial}{\partial x}\left(\Gamma_\epsilon\frac{\partial\epsilon}{\partial x}\right)+\frac{\partial}{\partial r}\left(r\Gamma_\epsilon\frac{\partial\epsilon}{\partial r}\right)+\frac{\partial}{r\partial\theta}\left(\Gamma_\epsilon\frac{\partial\epsilon}{r\partial\theta}\right)+\frac{C_1P\epsilon}{k}-\frac{C_2\rho\epsilon^2}{k} \quad (7)$$

The turbulent viscosity μ_t is calculated from the relation

$$\mu_t=C_\mu\rho k^2/\epsilon \quad (8)$$

The chemical reaction is assumed to be infinitely fast and to occur in one step. The combustion process is, therefore, limited by the mixing of the fuel stream and airstream. Further, because of the assumption of adiabatic flow, all properties can be related to a conserved scalar, defined as

$$f=\frac{\Phi-\Phi_A}{\Phi_F-\Phi_A} \quad (9)$$

where $\Phi=m_{\rm fu}-m_{\rm ox}/i$ (also a conserved scalar), and the subscripts F and A denote fuel stream and airstream, respectively. For an adiabatic flow, there is then no need for the solution of an enthalpy equation because the enthalpy equation is identical to the equation for the conserved scalar when both the variables are normalized between the fuel stream and the airstream. The statistical nature of the mixing is represented through an a priori probability density function. Transport equations for the mean (f) and variance (g) of the conserved scalar are solved.[6,7] These are

$$\frac{\partial}{\partial x}(\rho uf)+\frac{\partial}{r\partial r}(r\rho vf)+\frac{\partial}{r\partial\theta}(\rho wf)=\frac{\partial}{\partial x}\left(\Gamma_f\frac{\partial f}{\partial x}\right)+\frac{\partial}{\partial r}\left(r\Gamma_f\frac{\partial f}{\partial r}\right)+\frac{\partial}{r\partial\theta}\left(\Gamma_f\frac{\partial f}{r\partial\theta}\right) \quad (10)$$

$$\frac{\partial}{\partial x}(\rho ug)+\frac{\partial}{r\partial r}(r\rho vg)+\frac{\partial}{r\partial\theta}(\rho wg)=\frac{\partial}{\partial x}\left(\Gamma_g\frac{\partial g}{\partial x}\right)+\frac{\partial}{\partial r}\left(r\Gamma_g\frac{\partial g}{\partial r}\right)+\frac{\partial}{r\partial\theta}\left(\Gamma_g\frac{\partial g}{r\partial\theta}\right)+C_{g1}P_g-C_{g2}\frac{\rho\epsilon g}{k} \quad (11)$$

The various constants in the turbulence models are given the following values:

$$C_\mu=0.09,\ C_1=1.47,\ C_2=1.92,\ C_{g1}=2.8,\ C_{g2}=2.0$$
$$\sigma_\epsilon=1.3,\ \sigma_k=1.0,\ \sigma_f=0.6,\ \sigma_g=0.6 \quad (12)$$

The constants used here are those widely used in the literature and have been developed on the basis of comparisons in simple flow situations. Their accuracy in highly complex situations, such as the present one, remains to be demonstrated. However, for the present work, they appear to be the most appropriate values. The expressions for the additional source terms and the exchange coefficients are given in Table 1.

The fluid properties, such as density, specific heat, etc., are then evaluated from the temperature field that is calculated from the distribution of the mixture fraction and its variance.

Table 1 Exchange coefficients and additional source terms

ϕ	Γ_ϕ	S_ϕ
1	0	0
u	$\mu_\ell+\mu_t$	$\frac{\partial}{\partial x}\left(\mu_{\rm eff}\frac{\partial u}{\partial x}\right)+\frac{1}{r}\frac{\partial}{\partial r}\left(r\mu_{\rm eff}\frac{\partial v}{\partial x}\right)+\frac{1}{r}\frac{\partial}{\partial\theta}\left(\mu_{\rm eff}\frac{\partial w}{\partial x}\right)$
v	$\mu_\ell+\mu_t$	$\frac{\rho w^2}{r}+\frac{\partial}{\partial x}\left(\mu_{\rm eff}\frac{\partial u}{\partial r}\right)+\frac{1}{r}\frac{\partial}{\partial r}\left(r\mu_{\rm eff}\frac{\partial v}{\partial r}\right)+\frac{1}{r}\frac{\partial}{\partial\theta}\left(\mu_{\rm eff}r\frac{\partial}{\partial r}(w/r)\right)-2\frac{\mu_{\rm eff}}{r}\left(\frac{\partial w}{r\partial\theta}+\frac{v}{r}\right)$
w	$\mu_\ell+\mu_t$	$-\frac{\rho vw}{r}+\frac{\partial}{\partial x}\left(\mu_{\rm eff}\frac{\partial u}{r\partial\theta}\right)+\frac{\mu_{\rm eff}}{r}\left(r\frac{\partial(w/r)}{\partial r}+\frac{1}{r}\frac{\partial v}{\partial\theta}\right)+\frac{1}{r}\frac{\partial}{\partial\theta}\left(\mu_{\rm eff}\left(\frac{\partial w}{r\partial\theta}+\frac{2v}{r}\right)\right)+\frac{1}{r}\frac{\partial}{\partial r}\left(r\mu_{\rm eff}\left(\frac{1}{r}\frac{\partial v}{\partial\theta}-\frac{w}{r}\right)\right)$
k	$\mu_\ell+(\mu_t/\sigma_k)$	$0;\ P=\mu_t\left\{2\left(\frac{\partial u}{\partial x}\right)^2+2\left(\frac{\partial v}{\partial r}\right)^2+2\left(\frac{\partial w}{r\partial\theta}+\frac{v}{r}\right)^2+\left(\frac{\partial u}{\partial r}+\frac{\partial v}{\partial x}\right)^2+\left(\frac{\partial w}{\partial x}+\frac{\partial u}{r\partial\theta}\right)^2+\left(\frac{\partial v}{r\partial\theta}+\frac{\partial w}{\partial r}-\frac{w}{r}\right)^2\right\}$
ϵ	$\mu_\ell+(\mu_t/\sigma_\epsilon)$	0
f	$\mu_\ell+(\mu_t/\sigma_f)$	0
g	$\mu_\ell+(\mu_t/\sigma_g)$	$0;\ P_g=\mu_t\left\{\left(\frac{\partial f}{\partial x}\right)^2+\left(\frac{\partial f}{\partial r}\right)^2+\left(\frac{\partial f}{r\partial\theta}\right)^2\right\}$

A battlement-shaped probability density function is assumed and the maximum and minimum values of f at any point, f_+ and f_-, are presented by

$$f_+ = f + g^{1/2}, \qquad f_- = f - g^{1/2} \tag{13}$$

except where the value of f_+ exceeds unity and f_- is less than zero. In regions where f_+ exceeds unity and f_- is less than zero, a factor β is defined by

$$f = \beta f_+ + (1-\beta) f_- \tag{14}$$

where β represents the proportion of time spent in the f_+ state. Values of temperature and the mass fractions of fuel and oxygen are calculated corresponding to f_+ and f_-, and the mean quantities are obtained from the corresponding T_+, T_-, m_{fu_+}, m_{fu_-}, m_{ox_+}, and m_{ox_-} together with β. The density of the mixture of air, the combusting gas, and the combustion products is represented by the equation of a perfect gas:

$$\rho = Mp/RT \tag{15}$$

where M is the mixture molecular weight calculated from the relation

$$\frac{1}{M} = \frac{m_{\mathrm{fu}}}{M_{\mathrm{fu}}} + \frac{m_{\mathrm{ox}}}{M_{\mathrm{ox}}} + \frac{m_{\mathrm{pr}}}{M_{\mathrm{pr}}} \tag{16}$$

The mixture specific heat is calculated from a linear combination of the component specific heats. Thus,

$$C_p = \sum_i m_i C_{pi} \tag{17}$$

and

$$C_{pi} = a_i + b_i T + c_i T^2 \tag{18}$$

The stagnation enthalpy is defined as

$$h = m_{\mathrm{fu}} H_{\mathrm{fu}} + C_p T + \tfrac{1}{2}(u^2 + v^2 + w^2) \tag{19}$$

where H_{fu} is the heat of reaction. The values currently assigned to the constants in specific heat relations, molecular weights, etc., are given in Table 2 and correspond to those of gaseous ethylene (C_2H_4).

III. Solution Algorithm

The set of partial differential equations in Sec. II is solved by an iterative finite-difference algorithm, SIMPLE, developed by Patankar and Spalding.[8] The partial differential equations are integrated over small discrete regions called control volumes, and are converted to a set of nonlinear algebraic equations. The nonlinear algebraic equations are derived for the primitive variables u, v, w, and p. A staggered mesh system is employed in locating the flow variables on the finite-difference grid, and an exponential internode variation of the variable is assumed for the purpose of evaluating the fluxes from the faces of the control volumes.

Table 2 Fuel properties used[a]

Stoichiometric ratio, i			15.58
Heat of reaction, H_{fu}, kJ/kg			4.895×10^4
Molecular weights:			
Air			28.92
C_2H_4			28.0
Products			25.55
Specific heat constants, kJ/deg/kg:			
	a_i	b_i	c_i
Air	0.927	2.580×10^{-3}	3.820×10^{-8}
Fuel	0.404	4.360×10^{-3}	-1.353×10^{-6}
Products	0.918	8.415×10^{-4}	-2.12×10^{-7}

[a]The fuel properties correspond to those of C_2H_4.

The nonlinear algebraic equations are solved in a decoupled manner. The momentum equations are first solved using an estimated pressure field. The estimated pressure field is then updated by solving a pressure-correction equation, derived by combining the momentum and continuity equations. To prevent numerical instability, the successive changes of the flow variables are underrelaxed with their old values. The new value of a general variable, ϕ, is taken to be

$$\phi = \alpha\phi^n + (1-\alpha)\phi^o \tag{20}$$

where ϕ^n is the value computed with no underrelaxation and ϕ^o is the old iterative value. α is the underrelaxation factor which has a value between 0 and 1. The general structure of the final finite-difference equation is

$$A_P\phi_P = \sum_n A_n\phi_n + S^u + S^p\phi_P \tag{21}$$

where A_P and A_n are the finite-difference coefficients for point P and its six neighbors. S^u and S^p are the integrated source terms, S^p being the linearized part. Equation (21) is solved by repeated alternate line sweeps in the three coordinate directions. At each line, a line Gaussian elimination algorithm is used.

Complete details of the SIMPLE algorithm can be obtained from several earlier references, notably from Ref. 8. The momentum and continuity equations also can be solved in a fully coupled manner, resulting in a block implict method. Such an algorithm has been developed by Vanka[9] for two-dimensional flows and has been found to accelerate the convergence significantly. The block implicit algorithm has not yet been extended to three-dimensional flows.

IV. Calculated Flowfields and Scalar Fields

Computational Aspects

Because of the complexity of the flowfield, the rate of convergence of the calculations has been slow. For this reason, the present calculations were made only with a coarse finite-difference mesh consisting of a modest number (11 × 11 × 24) of grid nodes. Because of the symmetric flow, the equations were solved for only one-half of the cross section. The CPU time required for these calculations was 25 min on an IBM 3033 computer. Typically 450 iterations were necessary to make the residuals decrease to the 10^{-4} level. Because of the large computational times, finer finite-difference meshes could not be used. Nevertheless, the accuracy of the present calculations is sufficient to understand the flow processes in detail, and to draw conclusions about the trends of the influences of the various geometrical parameters.

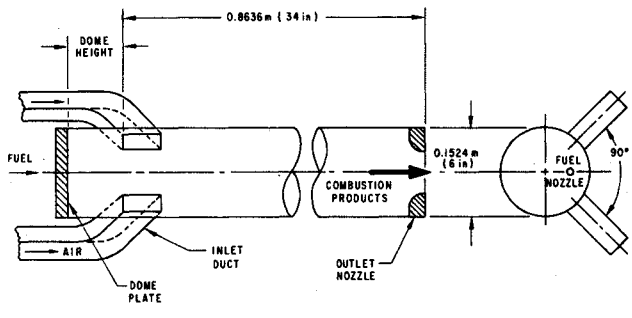

Fig. 1 Ducted rocket combustor configuration.

The conditions for the base configuration, given in Table 3, correspond to the combustor thrust stand.[2] Perturbations have been made to the base configuration to investigate the influence of the geometrical parameters. The results of the calculations are described in subsequent sections of this paper. Because of the limitations on the length of this paper, only a few results are presented. Complete details are given in Ref. 10.

Flowfield

The azimuthal location of the side arms and their inclination with the duct axis create a complex vortex pattern. In the cross stream, the flow consists of two symmetrical pairs of vortices. Figure 2 shows the development of these cross-sectional vortex structures at several axial distances of the base flow configuration. The vortex structures are more clearly formed downstream of the air entry, although some form of vortex structure is also observed in the dome region. The cross-stream vortex pattern observed in the reacting flow situation is similar to the isothermal flow pattern calculated earlier by Vanka et al.[3]

The flow structure in planes of constant azimuthal angle θ is shown in Fig. 3. The axial length is scaled down by a factor of 4. The flowfield in these planes consists basically of two regions. In the dome region, i.e., between the air inlets and the dome plate, the flow consists of low-velocity recirculating eddies. These eddies are formed through part of the airflow bifurcating into the dome region and interacting with the fuel stream. The flow in this region is truly three-dimensional. In the region downstream of the air inlet the flow is helical, being a superposition of a vortex pattern on an almost unidirectional flow. This flow structure of the azimuthal planes also is similar to the isothermal flowfield in Ref. 3, but some differences do exist. In the isothermal calculations, regions of flow recirculation were also observed downstream of the air inlet. These regions are absent in the reacting case. The probable cause for this is the expansion of the gases due to combustion, and the resulting higher flow velocities. It should be noted that although the flow in the region downstream of the air inlets is unidirectional, there can be significant flow ellipticities because of the nonuniformities in the pressure field.

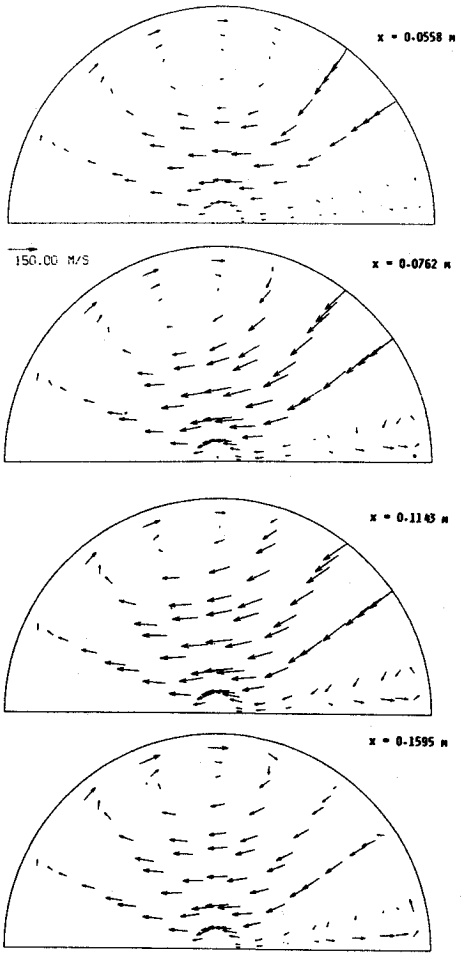

Fig. 2 Cross-stream flow patterns for base configuration.

Temperature and Fuel Fraction Contours

Figure 4 shows the contours of temperature at selected cross-sectional planes. Because of the diffusion flame assumption, the temperature patterns are linked closely to the fuel-air mixing patterns. The location where the fuel-air ratio is stoichiometric can be interpreted as being on the flame front. For the temperature contours, this corresponds to regions of steep temperature gradients.

Figure 4a corresponds to a location in the dome region. Here, the fuel jet is expanding and fuel-air mixing occurs at the boundary of the fuel jet. The location $x = 0.0889$ m (Fig. 4b) corresponds to the downstream edge of the air inlet. The air entry is from the right quadrant of the figure and is reflected in lower (~ 650 K) temperatures. The penetration of the airstream into the combusting mixture can be seen in Fig. 4c, characterized by lower temperatures. Figure 4d shows the temperature pattern that is formed after these complex mixing and reaction processes. The largest temperatures occur on the

Table 3 Conditions for base calculations

Diameter of combustor, m	0.1524
Length of combustor, m	0.8636
Dome height, m	0.0508
Angle of side arms, deg	45
Temperature of inlet air, K	556
Airflow rate (both arms), kg/s	1.814
Fuel flow rate ($F/A = 0.06$), kg/s	0.1088

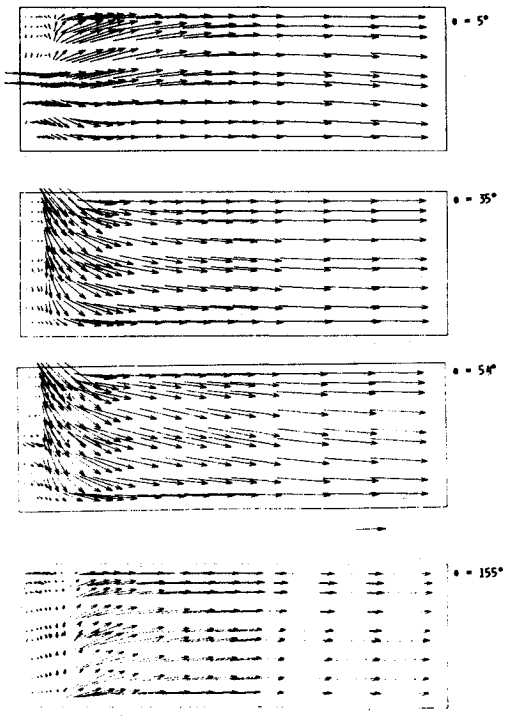

Fig. 3 Flow patterns in azimuthal planes for base configuration.

wall opposite to the airstream closer to the central plane, and near the fuel injection port. This behavior is in agreement with observed surface heating patterns.[2]

Figure 5 shows the contours of unburnt fuel fraction at various cross-sectional planes. The location of the fuel jet and its dispersal can be noticed easily from these plots. The region in the right quadrant of Fig. 5b corresponds to the air jet and has a low fuel fraction. The gradual mixing and dimunition of fuel along the ducted rocket can be seen from Figs. 5c and 5d. The fuel fractions are higher in the dome region because only a part of the airstream is bifurcated into the dome and is mixed with the fuel. For complete fuel-air mixing and no combustion, the fuel fraction would be 0.0566. Under conditions of complete combustion, there will be no fuel at the exit of the ducted rocket. In the present situation, some fuel still is present at $x=0.2540$ m, and even further (not shown here).

Figure 6 shows the cross-sectional average of unburnt fuel fraction plotted against the axial distance (the curves for other dome heights are discussed later). It is seen that the fuel fraction decreases very rapidly in the initial length of the ducted rocket. This region (up to $x\sim 0.3$ m) is characterized by intense turbulence and mixing. Beyond $x\sim 0.3$ m, the fuel-air mixing and reaction are slow, as reflected in the slow dimunition of the fuel. This slow rate of mixing is attributed to the nearly unidirectional flow shown earlier in Fig. 3. The combustion efficiency for this configuration is shown in Fig. 7. The combustion efficiency is defined as the ratio of actual enthalpy rise to the ideal value for complete combustion. The combustion efficiency for the present calculations is directly related to the mixing efficiency because of the diffusion flame assumption. These values compare very well with efficiencies observed in the thrust stand with combustor lengths of 0.762 and 0.457 m.

A few important conclusions can be drawn from the preceding plots. First, the flowfield in the ducted rocket is very complex, consisting of several recirculation eddies. These recirculation regions are advantageous for producing efficient fuel-air mixing. The flow in the downstream region, however, is almost unidirectional. Second, the temperature distribution in the cross section is severely nonuniform. In the case in which temperature-dependent finite chemical reaction rates are important, these nonuniformities can significantly influence the overall combustion efficiency. Third, about 60% of the efficiency is obtained in one-third of the length and the other 24% is recovered in the remaining two-thirds of the length. It is, therefore, desirable to investigate alternative configurations that will disturb the strong unidirectional flow. This might require major changes to the base configuration.

V. Influence of Geometrical Parameters

Several geometrical and flow parameters could influence the efficiency and the thrust produced by a ducted rocket. These include the dome height, angle of side arms, location of the fuel injector, fuel-air ratio, combustor pressure, and combustor dimensions. In this section the influence of the first three parameters is considered.

The location and angle of the side arms alter the flow patterns in the dome significantly. Vanka et al.[3] studied these patterns for the isothermal flow situation. It was observed that

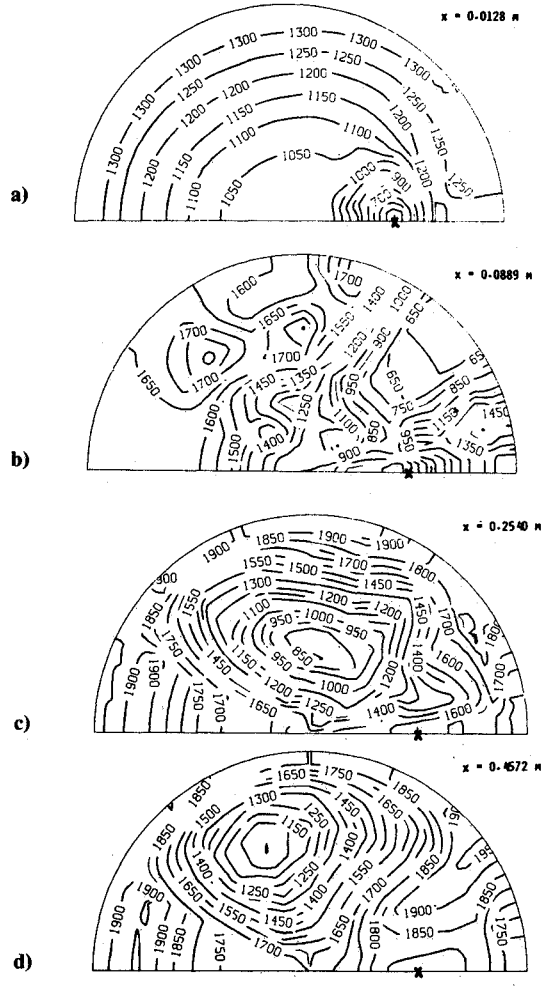

Fig. 4 Cross-stream temperature distribution for base configuration (X = location of fuel injector).

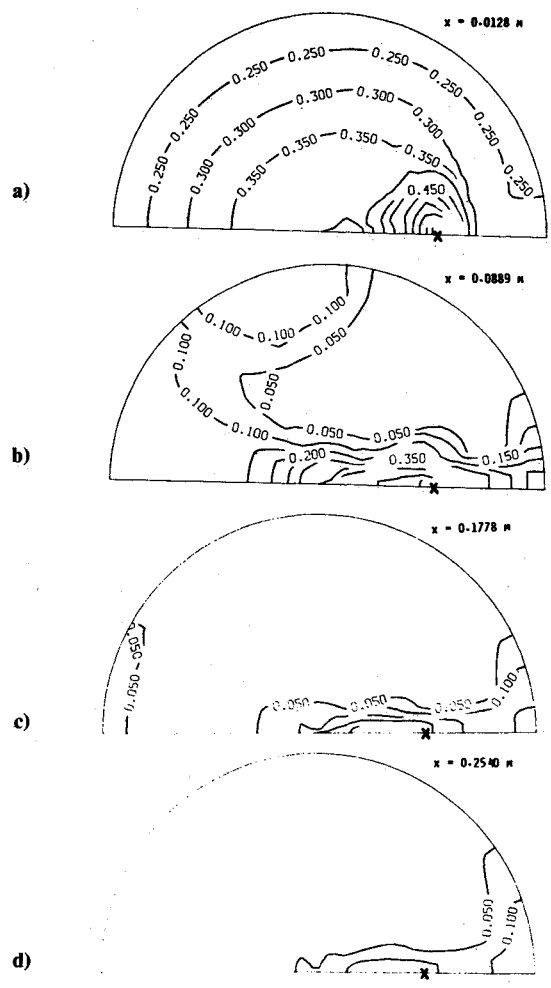

Fig. 5 Cross-stream fuel fraction distribution for base configuration (X = location of fuel injector).

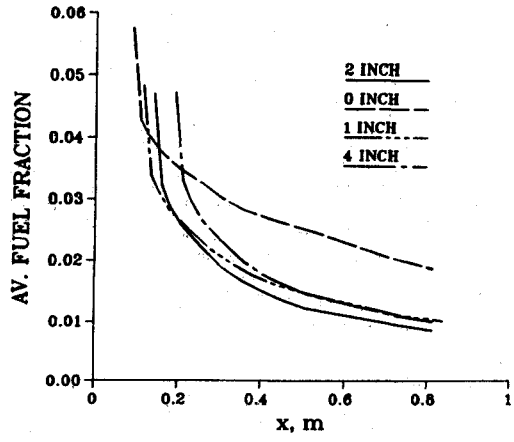

Fig. 6 Axial variation of fuel fraction for different dome heights.

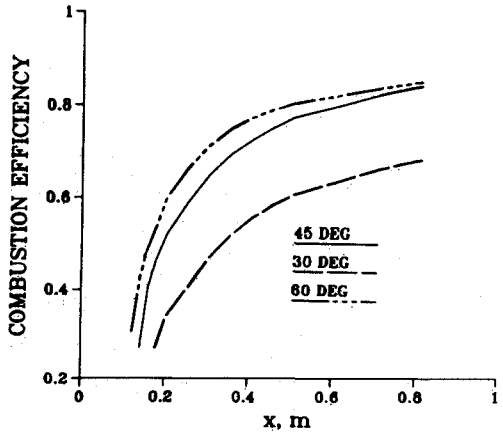

Fig. 8 Axial variation of combustion efficiency for different side-arm angles.

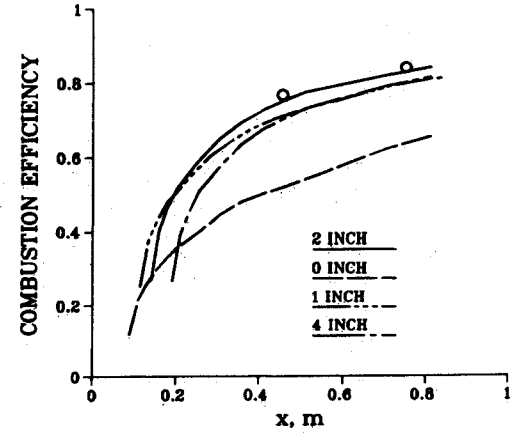

Fig. 7 Axial variation of combustion efficiency for different dome heights (o, Ref. 2 data).

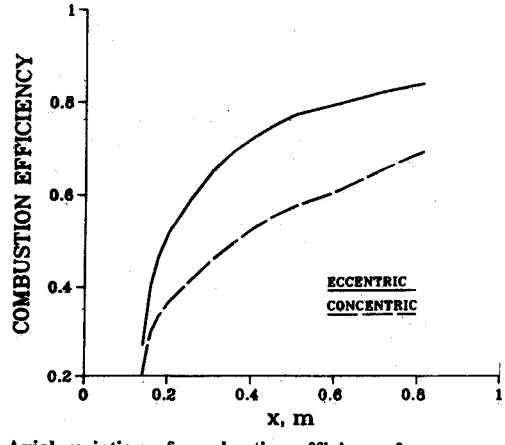

Fig. 9 Axial variation of combustion efficiency for concentric fuel injection.

shifting the side arms toward the dome plate compresses the eddy in the dome region, and steepening the angle of the arm modifies the recirculation pattern downstream of the airflow and in the dome region. In the present study, calculations have been made to examine the effect of these parameters in a reacting flow case. In addition, calculations are made with the fuel injector located at the center of the dome plate. The air- and fuel-flow rates and the inlet temperatures are held fixed. The effects of these parameters on the mixing and flow patterns are examined. Also, the average unburnt fraction is plotted against axial distance and is compared for the different cases.

Effect of Dome Height

The dome height influences the mixing process through changes to the recirculation flow in the dome region. At 0-m dome height (i.e., the side arms being flush with the dome plate), the recirculating flow in the dome region is markedly decreased and most of the air flows directly to the exit nozzle. The mixing is therefore significantly reduced. However, the cross-stream patterns are similar to the base case.

The average unburnt fuel fraction and the combustion efficiency for the various dome heights are shown in Figs. 6 and 7. Decreasing the dome height decreases combustion efficiency very little, except for the 0-m position. The decrease in combustion efficiency is directly related to the decrease in the recirculation eddy in the dome. Quite surprisingly, it is seen that the combustion efficiency is slightly lower for the dome height of 0.116 m. Apparently, the increased length of the dome region does not increase the bifurcating flow but decreases overall mixing because of the smaller combustor length available downstream of the air inlet. It is interesting to observe that the base configuration has the optimum dome height.

Effect of Side-Arm Angle

The inclination of the side arm with the duct axis influences the amount of fuel bifurcated into the dome region. The larger this bifurcation flow, the better the mixing. Steepening the side-arm angle increases the flow into the dome, thereby increasing the mixing.

This section examines the quantitative differences in mixing efficiency for three side-arm angles—60, 45 (base case), and 30 deg. The dome position and other parameters were held fixed at the base values. In Ref. 10 the detailed flow and temperature fields are presented; here only the effects on combustion efficiency are presented.

Figure 8 summarizes the effect of the side-arm angle through the plot of combustion efficiency along the combustor length. As expected, there is some improvement in the mixing efficiency when the angle of inclination is made steeper (to 60 deg), but flattening the angle (to 30 deg) lowers the efficiency considerably. These changes are purely the result of the modified flow paths and residence times.

Effect of Injector Location

The location of the injector alters the interface between the fuel stream and the airstream. We have compared here the fuel dispersal patterns for the cases of concentric and eccentric injection of the fuel. In the concentric case, the fuel injector is located at the center of the dome plate, and the other parameters are the same as the base case. The two flow patterns in the dome region are qualitatively different. In the con-

centric case, the fuel jet is in the region of the air impingement and interacts directly with the airstream. Therefore, the location of the flame front is also different in this case. The temperature contours for the concentric injection case are discussed in detail in Ref. 10.

Figure 9 shows combustion efficiency for the concentric injection case. The overall mixing efficiency has dropped to 70% from the base value of 84%. Although it was expected that the mixing efficiency might improve when the injector was located in the region of air impingement, it appears that the fuel jet has created a central adverse pressure gradient, thus decreasing the bifurcating airflow into the dome region. In the case of the eccentric injection, the fuel jet is not directly in the region where the airflow bifurcates, so more flow enters the dome, increasing the fuel-air mixing. This is an interesting observation, pointing out the importance of the bifurcating flow in improvement of the combustion efficiency.

VI. Summary

In this study we have analyzed the three-dimensional flowfield, fuel dispersal, and temperature distributions inside a ducted rocket configuration. The base calculations are made for a 0.1524-m-diam ducted rocket with 1.81 kg/s of air and burning ethylene at a fuel-air ratio of 0.06. The flow patterns, fuel fraction, and temperature contours are presented. The calculated overall combustion efficiency for the base configuration is in good agreement with the value measured in a thrust stand.[2] Unfortunately, there are no experimental data to compare the detailed three-dimensional flow and temperature variations. Such data will be helpful in validating the turbulence and combustion models used in this study.

The effects of the dome height, side-arm angle, and injector location are studied. These effects are examined through their impact on the residual fuel fraction and the combustion efficiency. It is observed that the 0.058-m dome height offers the best combustion efficiency compared with the 0-, 0.0254-, and 0.116-m positions. The mixing and consequent reaction are enhanced by steepening the side-arms angle, and are decreased when the fuel injector is located at the center of the dome plate rather than at an eccentric position.

Lastly, it should be mentioned that in the present study the effects of several factors, such as grid size, inlet turbulence levels, and turbulence model constants, have not been investigated thoroughly. Such studies must be undertaken in the future.

Acknowledgments

This work was performed at Argonne National Laboratory under the sponsorship of the Ramjet Technology Division, Wright-Patterson Air Force Base, through an interagency agreement.

References

[1]Streby, G. D., "Multi-ducted Inlet Combustor Research and Development," AFWAL-TR-83-2081, 1983.

[2]Stull, F. D., Craig, R. R., Streby, G. D., and Vanka, S. P., "Investigation of a Dual Inlet Side Dump Combustor Using Liquid Fuel Injection," *Journal of Propulsion and Power*, Vol. 1, Jan.-Feb. 1985, pp. 83-89.

[3]Vanka, S. P., Stull, F. D., and Craig, R. R., "Analytical Characterization of Flow Fields in Side Inlet Dump Combustors," AIAA Paper 83-0199, 1983.

[4]Chen, L. and Tao, C. C., "Study of Side-Inlet Dump Combustor of Solid Ducted Rocket with Reacting Flow," AIAA Paper 84-1378, 1984.

[5]Launder, B. E. and Spalding, D. B., "The Numerical Computation of Turbulent Flows," *Computer Methods in Applied Mechanics and Engineering*, Vol. 3, 1974, pp. 269-289.

[6]Spalding, D. B., "Concentration Fluctuations in a Round Turbulent Free Jet," *Chemical Engineering Science*, Vol. 26, 1971, pp. 95-107.

[7]Elgobashi, S. E. and Pun, W. M. "Concentration Fluctuations in Isothermal Turbulent Confined Coaxial Jets," *Chemical Engineering Science*, Vol. 32, 1977, pp. 161-166.

[8]Patankar, S. V. and D. B. Spalding, "A Calculation Procedure for Heat, Mass and Momentum Transfer in Three-Dimensional Parabolic Flows," *International Journal of Heat and Mass Transfer*, Vol. 15, 1972, pp. 1787-1806.

[9]Vanka, S. P., "Computations of Turbulent Recirculating Flows with Fully Coupled Solution of Momentum and Continuity Equations," Argonne National Laboratory, Argonne, IL, ANL-83-74, 1983.

[10]Vanka, S. P., Craig, R. R., and Stull, F.D., "Mixing, Chemical Reaction, and Flow Field Development in Ducted Rockets," Argonne National Laboratory, Argonne, IL, ANL-84-62, 1984.